

Thermodynamic theory of crystal plasticity: formulation and application to polycrystal fcc copper

Charles K. C. Lieou^a, Curt A. Bronkhorst^{a,b,*}

^a*Theoretical Division, Los Alamos National Laboratory, Los Alamos, NM 87545, USA*

^b*Department of Engineering Physics, University of Wisconsin-Madison, Madison, WI 53706, USA*

Abstract

We present a thermodynamic description of crystal plasticity. Our formulation is based on the Langer-Bouchbinder-Lookman thermodynamic dislocation theory (TDT), which asserts the fundamental importance of an effective temperature that describes the state of configurational disorder and therefore the dislocation density of the crystalline material. We extend the TDT description from isotropic plasticity to crystal plasticity with many slip systems. Finite-element simulations show favourable comparison with experiments on polycrystal fcc copper under uniaxial compression, tension, and simple shear. The thermodynamic theory of crystal plasticity thus provides a thermodynamically consistent and physically rigorous description of dislocation motion in crystals. We also discuss new insights about the interaction of dislocations belonging to different slip systems.

Keywords: Constitutive behavior, Crystal plasticity, Copper, Finite-element simulation, Taylor-Quinney coefficient

1. Introduction

The topic of representation of the mechanics and especially thermodynamics of dislocation motion and interaction remain areas of strong scientific and technological interest (e.g., Gurtin et al., 2010; Kubin, 2013; Bulatov and Cai,

*Corresponding author

Email address: cbronkhorst@wisc.edu (Curt A. Bronkhorst)

¹LA-UR release number: LA-UR-19-31861

2007; Clayton, 2011). In particular, significant questions and opportunities remain in understanding and quantifying material hardening, dislocation structure development, and deformation energy partitioning. Although challenges remain in experimental quantification of dislocation behavior, new lower length scale techniques offer important new opportunities to gather physical insight on dislocation behavior (e.g., Pathak and Kalidindi, 2015; Thevamaran et al., 2016; Pathak et al., 2012; Xue et al., 2017; Brown et al., 2017; Upadhyay et al., 2014; Gigax et al., 2019). Of equal importance are the many contributions made to define not only the kinematics of dislocation motion but also the energy states within thermodynamically consistent theories and computational frameworks (e.g., Berdichevsky, 2006, 2017, 2018b,a, 2019a,b; Anand et al., 2015; Le, 2018, 2019; Hochrainer, 2016; Levitas and Javanbakht, 2015b; Arora and Acharya, 2019; Po et al., 2019; Chowdhury and Roy, 2019; Jiang et al., 2019; Nieto-Fuentes et al., 2018; Jafari et al., 2017; Shizawa et al., 2001; del Castillo and Huang, 2012; Langer et al., 2010; Langer, 2015; Roy and Acharya, 2005, 2006; Acharya, 2010). Recent work (Berdichevsky, 2019a) has pointed out statements of discouragement from the community in relationship to the difficulty of understanding and quantifying work hardening in metallic materials. Although difficult, the topic continues to be one of high economic and strategic value requiring models which are dedicated to specific materials (Berdichevsky, 2019a). Due to cumulative history effects and structural evolution, quantifying the details of the dislocation (and deformation twinning) mediated plasticity will be critical in predicting the ductile based damage of materials (Boyce et al., 2014, 2016). Especially with regards to material damage, the ability to successfully predict when and where materials fail will require theories specified by material and properly account for energy and thermodynamic coupling between the different deformation mechanisms.

Early work in crystal plasticity theory had as a focus the structural representation of materials and the influence of the kinematics of discrete close-packed slip systems on crystallographic rotation and the development of crystallographic texture with deformation (e.g., Hill and Rice, 1972; Asaro and Rice, 1977; Asaro, 1983b,a; Asaro and Needleman, 1985). This large-deformation kinematical framework for models was an important element of enabling the prediction of crystallographic texture development (Harren and Asaro, 1989; Harren et al., 1989; Wu et al., 1991; Bassani and Wu, 1991; Bassani, 1993; Bronkhorst et al., 1992; Kalidindi et al., 1992). The crystallographic rotations had a close relationship with the imposed mode of deformation and de-

pendence upon material type. The imprinting of crystallographic symmetries on macro-scale behaviors via granular rotations has significant implication for component manufacturing and material processing. This continues to be a very important area of application. The use of X-ray diffraction techniques supplementing mechanical testing enabled the study of preferred orientation of materials during large deformation and provided important experimental data to compare with simulations using these classical single crystal theories and homogenization techniques (Bunge, 1982; Kocks et al., 1989). The years of work in developing homogenization strategies for engineering scale simulations of large deformation problems also inferred the importance of intergranular interactions (e.g., Houtte et al., 2005; Houtte, 1982, 1988; Lebensohn and Tome, 1993; Bronkhorst et al., 1992; Kalidindi et al., 1992; Lebensohn, 2001). Incorporating rate dependence in deformation also provided a natural selection process for dominant slip systems and remains an important element of most models (Peirce et al., 1982, 1983; Asaro and Needleman, 1985). The models discussed here established the early kinematical and computational foundations but did not comprehensively account for energy considerations or thermodynamics of plastic processes.

With an eye towards greater abilities to predict the deformation response of metallic materials, there has been a systematic drive towards greater physical basis of continuum crystal models. Although dislocation motion is inherently discrete at the length scale of the Burgers vector, there have been many critical advances in continuum dislocation mechanics theories (Arsenlis and Parks, 1999, 2002; Gurtin, 2000; Gurtin and Needleman, 2005; Acharya et al., 2004; Anand et al., 2005; Busso and McClintock, 1996; Busso et al., 2000; Aifantis, 1992; Fleck and Hutchinson, 1993, 1997; Zhu et al., 1995; Gerken and Dawson, 2008; Mayeur et al., 2011; Mayeur and McDowell, 2015) employing high level dislocation mechanics representations. More recently, theories for advanced representation of dislocation interaction and reactions have been formed and quantified using techniques of molecular dynamics and discrete dislocation dynamics (e.g., Kubin, 2013; Bulatov and Cai, 2007; Zepeda-Ruiz et al., 2017). Given the relative simplicity of face-centered-cubic structures, advances in continuum representation of these materials have been more straightforward relative to BCC and HCP structures. A key advancement has been the move from a scalar representation of forest hardening to that of tensorial representation of specific slip system interactions and reactions (Madec et al., 2002, 2003; Devincre et al., 2006, 2008; Grilli et al., 2018; Dequiedt et al., 2015; Hansen et al., 2013). The work of Hansen et al.

(2013) in particular includes non-mobile populations of dislocations which are sources of internal stored energy. In fact, some work suggests that dislocation sub-cell development is a result of lowering overall system energy (e.g., Hansen et al., 2010) and these continuum formulations have been used to study dislocation structural development during deformation at high resolutions (Dequiedt et al., 2015; Grilli et al., 2018; Arora and Acharya, 2019).

It has been known for some time that dislocation mediated plasticity is energy dissipative and a significant increase of temperature is possible (Farren and Taylor, 1925; Taylor and Quinney, 1934), especially when deformation is large and there is inadequate time for thermal transport to dissipate the energy. The proportion of plastic work transformed to thermal energy remains a very important area of research and is of technological interest to the processing of materials and material energy dissipation applications. For many types of loading conditions, the energy state of the material is an important state variable and the energy partitioned for dislocation state evolution must be considered (e.g., Feng et al., 2019; Wu et al., 2003; Mourad et al., 2017; Luscher et al., 2018; Barton et al., 2005; Feng and Bronkhorst, 2019; Vogler and Clayton, 2008; Levitas et al., 2006; Levitas and Javanbakht, 2015b). Despite more recent experimental work found in literature (Marchand and Duffy, 1988; Hartley et al., 1987; Duffy and Chi, 1992; Rittel et al., 2012, 2017) thermometry remains challenging to perform accurately and more experimental work is required. This body of work strongly suggests that the Taylor-Quinney coefficient (Taylor and Quinney, 1934) is not a constant value as is commonly assumed (e.g., Bronkhorst et al., 2016) but can evolve significantly in magnitude with deformation. Recent work also suggests that the Taylor-Quinney coefficient differs in magnitude between slip and twinning processes (Kingstedt and Lloyd, 2019). Together with the complexity of continuum descriptions of the mechanics of dislocation motion and interactions, theoretical development is also an active research area (Zehnder, 1991; Rosakis et al., 2000; Benzerga et al., 2005; Longère and Dragon, 2008b,a; Stainier and Ortiz, 2010; Zaera et al., 2013; Anand et al., 2015; Luscher et al., 2018; Nieto-Fuentes et al., 2018).

In the context of high deformation rate loading, we have proposed a novel thermodynamic description of structural evolution taking place during deformation (Lieou and Bronkhorst, 2018; Lieou et al., 2019). This approach is based upon recent work to partition energy and entropy elements to both atomic vibrational and atomic disorder states of matter (Langer et al., 2010; Langer, 2015). This general theory based upon atomic scale principles

then provides a disciplined thermodynamic framework to describe structural features such as dislocations, dislocation subcells, grain boundaries, and so on. In our prior work (Lieou and Bronkhorst, 2018; Lieou et al., 2019) and other recent applications of this theory (Langer, 2016, 2017a,b; Le et al., 2018; Le, 2018, 2019) the atomic disorder component or dislocation, subcell, grain boundary representation was done only through isotropic and scalar representations of these states. There was but one dislocation density and grain boundary density measure used in the theory and subsequent simulations of experimental results. Here we advance upon the work in (Lieou and Bronkhorst, 2018; Lieou et al., 2019) by applying this general thermodynamic approach to an advanced continuum theory of single crystal behavior for FCC systems. In this way, we significantly advance the description of the disorder (structure) partition component applied to specific crystallographic structure and begin to address the challenging questions raised above (Berdichevsky, 2006, 2017, 2018b,a, 2019a,b; Anand et al., 2015; Le, 2018, 2019; Hochrainer, 2016; Levitas and Javanbakht, 2015a; Arora and Acharya, 2019; Po et al., 2019; Chowdhury and Roy, 2019; Jiang et al., 2019; Nieto-Fuentes et al., 2018; Jafari et al., 2017; Shizawa et al., 2001; del Castillo and Huang, 2012; Langer et al., 2010; Langer, 2015; Roy and Acharya, 2005, 2006; Acharya, 2010).

This paper is structured as follows. In Sec. 2, we present a crystal-plasticity formulation of the TDT, appropriately accounting for finite deformation and the resolution into different slip planes. We briefly discuss the computational method in Sec. 3. We validate our thermodynamic crystal-plasticity framework by direct comparison to a set of uniaxial compression experiments on copper in Sec. 4, and validate model results against simple shear and uniaxial tension in Sec. 5. We discuss some outstanding problems in Sec. 6 and conclude the paper in Sec. 7. The nomenclature and quantities used within are given below in Table 1.

2. Thermodynamic theory of dislocation plasticity: a crystal-plasticity formulation

2.1. Crystal plasticity and deformation kinematics

As in conventional crystal plasticity formulations, the deformation gradient \mathbf{F} can be decomposed (Kroner, 1960) into elastic and plastic contributions, \mathbf{F}^e and \mathbf{F}^p :

$$\mathbf{F} = \mathbf{F}^e \mathbf{F}^p. \quad (1)$$

Table 1: List of symbols

Symbol	Definition or meaning
$\mathbf{F}, \mathbf{F}^e, \mathbf{F}^p$	Total, elastic, and plastic deformation gradients
$\mathbf{L}, \mathbf{L}^e, \mathbf{L}^p$	Total, elastic, and plastic velocity gradients
$\dot{\gamma}^\alpha$	Resolved plastic strain rate on slip system α
$\mathbf{s}^\alpha, \mathbf{m}^\alpha$	Unit slip direction vector and normal to slip system α
σ	Cauchy stress tensor
\mathbf{S}	Second Piola-Kirchhoff stress tensor
\mathbf{C}	Anisotropic fourth-order tensor of elastic constants
C_{11}, C_{12}, C_{44}	Independent crystallographic moduli for fcc lattice
μ	Shear modulus
\mathcal{W}	Jacobian matrix of stress versus strain
$U_{\text{tot}}, S_{\text{tot}}$	Total energy and entropy density
U_K, S_K	Kinetic-vibrational (thermal) energy and entropy density
U_C, S_C	Configurational energy and entropy density
U_D, S_D	Dislocation energy and entropy
U_1, S_1	Residual configurational energy and entropy density
F_C	Configurational free energy density
e_D	Dislocation line energy
χ	Effective temperature
θ, T	Thermal temperature (in units of energy and Kelvin)
ρ_{ss}^α	Steady-state dislocation density on slip system α
χ_{ss}	Steady-state effective temperature (in units of e_D)
c_p	Specific heat capacity
κ_ρ^α	Dislocation storage rate
κ_χ	Effective temperature increase rate
a	Minimum separation between dislocations
b	Burgers vector
t_0	Atomic time scale
α_T	Stress scale parameter
τ^α	Resolved shear stress on slip system α
s_T^α	Slip resistance on slip system α
ρ^α	Dislocation density corresponding to slip system α
l^α	Dislocation mean free path on slip system α
t^α	Dislocation depinning time on slip system α
T_P	Dislocation depinning barrier (in units of Kelvin)
$a^{\alpha\beta}, f^{\alpha\beta}$	Dislocation interaction tensors
$d^{\alpha\beta}$	Slip interaction tensor
e_N	Interaction energy scale between dislocations on different slip systems
k_c, k_{nc}	Mean free path parameters

Plastic velocity gradient is derived from the plastic shear strain rate on close-packed dislocation slip systems indexed by α :

$$\mathbf{L}^p \equiv \dot{\mathbf{F}}^p (\mathbf{F}^p)^{-1} = \sum_{\alpha} \dot{\gamma}^{\alpha} \mathbf{s}^{\alpha} \otimes \mathbf{m}^{\alpha}, \quad (2)$$

where \mathbf{s}^{α} is the unit slip direction vector, \mathbf{m}^{α} is the unit normal to the slip plane vector α , and $\dot{\gamma}^{\alpha}$ is the plastic strain rate on slip system α , all defined in the reference configuration. If \mathbf{S} is a stress tensor of the second Piola-Kirchhoff type, defined by

$$\mathbf{S} \equiv J (\mathbf{F}^e)^{-1} \boldsymbol{\sigma} (\mathbf{F}^e)^{-T}, \quad (3)$$

where $\boldsymbol{\sigma}$ is the Cauchy stress tensor, and $J = \det \mathbf{F} = \det \mathbf{F}^e$ is the Jacobian of the transformation between the reference and deformed configurations (the second inequality holds because we assume plastic incompressibility, $\det \mathbf{F}^p = 1$), then the resolved shear stress τ^{α} on slip system α is given by

$$\tau^{\alpha} = (\mathbf{F}^e)^T \mathbf{F}^e \mathbf{S} : (\mathbf{s}^{\alpha} \otimes \mathbf{m}^{\alpha}) \approx \mathbf{S} : (\mathbf{s}^{\alpha} \otimes \mathbf{m}^{\alpha}), \quad (4)$$

where the approximation follows because elastic strains for conditions of loading considered in this work are small. The resolved shear stress thus defined provides a simple expression for the total plastic work rate:

$$\boldsymbol{\sigma} : \mathbf{F}^e \mathbf{L}^p (\mathbf{F}^e)^{-1} = \sum_{\alpha} \tau^{\alpha} \dot{\gamma}^{\alpha}, \quad (5)$$

the right-hand side being the sum of the plastic work rates on all slip systems.

2.2. Stress response

The second Piola-Kirchhoff stress tensor \mathbf{S} is related to the elastic part of the deformation gradient \mathbf{F}^e by

$$\mathbf{S} = \frac{1}{2} \mathbf{C} ((\mathbf{F}^e)^T \mathbf{F}^e - \mathbf{I}), \quad (6)$$

where \mathbf{C} is the anisotropic fourth-order tensor of elastic constants. For cubic crystallographic systems, this tensor is composed of three independent moduli in C_{11} , C_{12} , and C_{44} .

2.3. Thermodynamics and state variable evolution

As in many conventional theories of dislocation plasticity (e.g., Cheong and Busso, 2004; Hansen et al., 2013; Anand et al., 2015; Dequiedt et al., 2015; Zecevic et al., 2015; Knezevic and Beyerlein, 2018; Bronkhorst et al., 2019), the relevant internal state variable is the dislocation density ρ^α on the different slip systems α . What distinguishes the present approach from conventional theories is that the evolution of the dislocation density are derived from energetic and entropic considerations alone, subject to the constraints of the first and second laws of thermodynamics. Our derivation here is largely parallel to that described in simpler and isotropic set-ups (e.g., Langer et al., 2010; Langer, 2015; Lieou and Bronkhorst, 2018; Lieou et al., 2019), but is now adapted to incorporate finite deformation and different slip systems with some initial accounting for dislocation interactions.

Let U_{tot} and S_{tot} denote the total energy and entropy density per unit volume of the material, each being a sum of kinetic-vibrational (i.e., thermal motion of atoms) and configurational (i.e., positions of atoms, defects, etc.) contributions:

$$U_{\text{tot}} = U_K + U_C; \quad S_{\text{tot}} = S_K + S_C. \quad (7)$$

U_C and S_C are clearly functions of relevant internal state variables and, in particular, of the dislocation densities ρ^α , so that

$$U_C(S_C, \rho^\alpha) = U_D(\rho^\alpha) + U_1(S_1); \quad (8)$$

$$S_C(U_C, \rho^\alpha) = S_D(\rho^\alpha) + S_1(U_1). \quad (9)$$

where U_D and S_D denote contributions from dislocations, and U_1 and S_1 are the residual configurational energy and entropy densities for all other configurational degrees of freedom (e.g., impurities, point defects). An important quantity to our theoretical development is the effective temperature defined as

$$\chi \equiv \frac{\partial U_C}{\partial S_C}, \quad (10)$$

which quantifies the atomic disorder in the material relative to the perfect crystal.

Before specifying the dependence of U_C and S_C on the dislocation densities ρ^α , let us first examine the consequences of the laws of thermodynamics.

The first law of thermodynamics says that

$$\begin{aligned}\dot{U}_{\text{tot}} &= \boldsymbol{\sigma} : \mathbf{L} = \dot{U}_C + \dot{U}_K \\ &= \chi \dot{S}_C + \left(\frac{\partial U_C}{\partial t} \right)_{S_C, \rho^\alpha} + \sum_\alpha \left(\frac{\partial U_C}{\partial \rho^\alpha} \right)_{S_C} \dot{\rho}^\alpha + \theta \dot{S}_K,\end{aligned}\quad (11)$$

where $\theta = k_B T$ is the ordinary, thermal temperature in energy units (k_B being the Boltzmann constant), and $\mathbf{L} = \dot{\mathbf{F}} \mathbf{F}^{-1}$ is the velocity gradient, which can be separated into elastic and plastic contributions:

$$\mathbf{L} = \mathbf{L}^e + \mathbf{F}^e \mathbf{L}^p (\mathbf{F}^e)^{-1}, \quad (12)$$

with $\mathbf{L}^e = \dot{\mathbf{F}}^e (\mathbf{F}^e)^{-1}$, and \mathbf{L}^p given above in Eq. (2). Observe now that

$$\left(\frac{\partial U_C}{\partial t} \right)_{S_C, \rho^\alpha} = \boldsymbol{\sigma} : \mathbf{L}^e \quad (13)$$

because deformation at fixed configurational state is elastic by definition. Thus

$$\boldsymbol{\sigma} : \mathbf{F}^e \mathbf{L}^p (\mathbf{F}^e)^{-1} = \chi \dot{S}_C + \sum_\alpha \left(\frac{\partial U_C}{\partial \rho^\alpha} \right)_{S_C} \dot{\rho}^\alpha + \theta \dot{S}_K, \quad (14)$$

Turn now to the second law of thermodynamics, which states that

$$\dot{S}_{\text{tot}} = \dot{S}_C + \dot{S}_K \geq 0. \quad (15)$$

Multiplying this by χ , and eliminating \dot{S}_C using Eq. (14) above, we get

$$\boldsymbol{\sigma} : \mathbf{F}^e \mathbf{L}^p (\mathbf{F}^e)^{-1} - \sum_\alpha \left(\frac{\partial U_C}{\partial \rho^\alpha} \right)_{S_C} \dot{\rho}^\alpha + (\chi - \theta) \dot{S}_K \geq 0. \quad (16)$$

According to the Coleman-Noll procedure (Coleman and Noll, 1963), each independently variable term must be non-negative in order for the overall inequality to hold. This follows automatically for the plastic work term (see Eq. (5) above). Thus we arrive at the constraints

$$- \left(\frac{\partial U_C}{\partial \rho^\alpha} \right)_{S_C} \dot{\rho}^\alpha \geq 0; \quad (\chi - \theta) \dot{S}_K \geq 0. \quad (17)$$

The second of these inequalities constrains the Taylor-Quinney factor which determines the amount of plastic power that goes into heating up the material, as has been discussed in Lieou et al. (2019). The implications of the

first inequality can be seen by writing $U_C(S_C, \rho^\alpha) = U_D(\rho^\alpha) + U_1(S_1) = U_D(\rho^\alpha) + U_1(S_C - S_D(\rho^\alpha))$, from which it follows that

$$\left(\frac{\partial U_C}{\partial \rho^\alpha}\right)_{S_C} = \frac{\partial U_D}{\partial \rho^\alpha} - \chi \frac{\partial S_D}{\partial \rho^\alpha} \equiv \frac{\partial F_C}{\partial \rho^\alpha}, \quad (18)$$

where

$$F_C(\rho^\alpha) = U_D(\rho^\alpha) - \chi S_D(\rho^\alpha) \quad (19)$$

is the configurational free energy density. (The second term in the first equality in Eq. (18) follows from a direct application of the chain rule of differential calculus to U_1 and the definition of χ). Thus the first of Eq. (17) implies that deformation causes the material to dynamically minimize its configurational free energy. In addition, the material reaches its non-equilibrium steady state, i.e., $\dot{\rho}^\alpha = 0$, when $\partial F_C / \partial \rho^\alpha = 0$. This non-equilibrium steady state is possible when the rate of dislocation generation due to multiplication processes balance the rate of dislocation annihilation due to interaction processes. This means that the steady state dislocation densities ρ_{ss}^α can be obtained by locating configurational free energy minima which are generally a function of material state and loading conditions.

The entropy density S_D can be computed by directly counting the microstates across slip systems (e.g., Lieou and Bronkhorst (2018)); the result is

$$S_D = \frac{1}{a} \sum_{\alpha} [-\rho^\alpha \ln(a^2 \rho^\alpha) + \rho^\alpha]. \quad (20)$$

where the quantity a is an atomic length scale, not necessarily the Burgers vector magnitude b . We shall specify the corresponding dislocation energy density U_D shortly afterwards when we specify the interaction between different slip systems in Sec. 2.4.

Based on energetic considerations alone, the evolution of the dislocation density must be proportional to the rate at which input work is stored in newly formed dislocations, which in turn is proportional to the plastic work rate. This contrasts with conventional crystal plasticity theories, according to which the dislocation density evolves at a rate proportional to the absolute value of the slip rate of the corresponding slip system. Thus our proposed evolution equation for ρ^α is of the form

$$\dot{\rho}^\alpha = \frac{\kappa_\rho^\alpha}{a^2} \frac{\tau^\alpha \dot{\gamma}^\alpha}{\mu} \left(1 - \frac{\rho^\alpha}{\rho_{ss}^\alpha}\right). \quad (21)$$

Equation (21), as written, explicitly assumes that dislocation creation on a given slip system is driven only by plastic slip on that system. This is the case for conventional dislocation theories as well (e.g., Cheong and Busso, 2004; Hansen et al., 2013; Anand et al., 2015; Dequiedt et al., 2015; Zecevic et al., 2015; Knezevic and Beyerlein, 2018; Bronkhorst et al., 2019). Here, κ_ρ^α is a dynamic parameter that controls the hardening rate; μ , the shear modulus and only relevant stress scale for deviatoric deformation, is inserted in the denominator for dimensional consistency.

The effective temperature χ follows an evolution equation of the form

$$\frac{\dot{\chi}}{e_D} = \kappa_\chi \frac{\sum_\beta \tau^\beta \dot{\gamma}^\beta}{\mu} \left(1 - \frac{\chi}{\chi_{ss}} \right), \quad (22)$$

where κ_χ is a dimensionless parameter, and χ_{ss} is the steady-state effective temperature, which may be strain-rate dependent. Finally, if there is no heat exchange with the surroundings and conditions can be assumed to be adiabatic, the thermal temperature evolves according to

$$\dot{T} = \frac{\beta_T}{\bar{\rho}_M c_p} \sum_\beta \tau^\beta \dot{\gamma}^\beta, \quad (23)$$

where $\beta_T \approx \chi/\chi_{ss}$, the Taylor-Quinney coefficient, quantifies the fraction of plastic power converted into heat. $\bar{\rho}_M$ is the mass density of the material, and c_p is the specific heat capacity of the material per unit mass. At fast loading rates, one can assume adiabatic deformation, and neglect the exchange of heat with the surroundings and the flow of heat across the material. At quasistatic loading rates, one can assume isothermal conditions and neglect the temporal evolution of T .

2.4. Kinematics of dislocations and interaction between different slip systems

To complete our theoretical description we need an expression for the plastic strain rate $\dot{\gamma}^\alpha$ on slip system α . This is given by the Orowan relation:

$$\dot{\gamma}^\alpha = \rho^\alpha b v^\alpha, \quad (24)$$

where v^α is the average dislocation speed on slip system α .

We regard dislocation motion as a stress-driven, thermally-activated depinning process that takes place on a time scale t^α given by

$$\frac{1}{t^\alpha} = \frac{1}{t_0} \exp \left(-\frac{T_P}{T} e^{-\tau^\alpha/s_T^\alpha} \right), \quad (25)$$

where T is the temperature in units of Kelvin, and T_P characterizes the depinning energy barrier through the product $k_B T_P$ with the Boltzmann constant k_B , and s_T^α the slip resistance on slip system α . As is commonly done, if l^α denotes the mean-free path of a single dislocation in slip system α in the dislocation forest, one would expect that $v^\alpha = l^\alpha/t^\alpha$, so that

$$\dot{\gamma}^\alpha = \frac{\rho^\alpha l^\alpha b}{t_0} \exp\left(-\frac{T_P}{T} e^{-\tau^\alpha/s_T^\alpha}\right). \quad (26)$$

In the scalar, isotropic version of the TDT, the expressions for the mean-free path and the slip resistance are relatively simple: $l = 1/\sqrt{\rho}$ and $s_T \propto \sqrt{\rho}$, where we suppress the slip system index α because of its irrelevance. Also, the dislocation energy density U_D discussed above in Sec. 2.3 is linear in the dislocation density in the non-interacting approximation: $U_D = \frac{e_D \rho}{a}$. All of these, however, are places where interaction between slip systems could come into play in the present crystal-plasticity formulation. Specifically,

1. The slip resistance, or the Taylor stress, could couple the dislocation densities ρ^α corresponding to the different slip systems, for dislocation motion is impeded by the dislocation forest itself:

$$s_T^\alpha = \alpha_T \mu b \sqrt{\sum_\beta a^{\alpha\beta} \rho^\beta}, \quad (27)$$

where $a^{\alpha\beta}$ is a dislocation interaction tensor. The scaling factor α_T is inserted in light of the uncertainty between the stress barrier for traditional theories documented in the literature (e.g., Hansen et al., 2013), and the stress barrier in the present theory.

2. The mean-free path of a dislocation in slip system α could depend on the dislocation densities in other slip systems of the dislocation forest:

$$l^\alpha = \frac{1}{\sqrt{\sum_\beta d^{\alpha\beta} \rho^\beta}}, \quad (28)$$

where $d^{\alpha\beta}$ is the slip interaction tensor.

3. The dislocation formation energy U_D could contain an interaction term that couples the different systems:

$$U_D(\rho^\alpha) = \frac{1}{a} \left(\sum_\alpha e_D \rho^\alpha + \frac{b^2 e_N}{2} \sum_\alpha \sum_\beta f^{\alpha\beta} \rho^\alpha \rho^\beta \right), \quad (29)$$

where $f^{\alpha\beta}$ is yet another dislocation interaction tensor, and e_N is an interaction energy scale. With the entropy S_D given in Eq. (20), the steady-state dislocation energy density is given by

$$\rho_{\text{ss}}^\alpha = \frac{1}{a^2} \exp \left(-\frac{e_D + b^2 e_N \sum_\beta f^{\alpha\beta} \rho^\beta}{\chi} \right). \quad (30)$$

This expression implies the interesting possibility that an accumulation of dislocations in some slip planes could cause a reduction of the dislocation density in other slip planes.

Possibilities 1 and 2 have direct counterparts in conventional dislocation theories such as theories of the Kocks-Mecking type (e.g., Mecking and Kocks, 1981), and appear to give us better fits to the copper stress-strain data that the present manuscript is concerned with. Setting the dislocation interaction energy equal to zero gives a simple expression for the steady-state dislocation density:

$$\rho_{\text{ss}}^\alpha = \frac{1}{a^2} e^{-e_D/\chi}. \quad (31)$$

However, possibility 3 – a non-trivial interaction energy between different slip systems – remains an interesting prospect, which we intend to address in future work. From here onwards, we adopt units in which $e_D = 1$, and render χ dimensionless.

With these ingredients, the slip rate is given by

$$\dot{\gamma}_{|\tau^\alpha|>0}^\alpha = \frac{\bar{\rho}^\alpha}{t_0 \sqrt{\sum_\beta d^{\alpha\beta} \bar{\rho}^\beta}} \exp \left[-\frac{T_P}{T} e^{-\tau^\alpha/(\mu \sqrt{\sum_\beta a^{\alpha\beta} \bar{\rho}^\beta})} \right] \equiv \frac{f(\tau^\alpha, \bar{\rho}^\alpha)}{t_0}, \quad (32)$$

where $\bar{\rho}^\alpha \equiv b^2 \rho^\alpha$ is the rescaled, dimensionless dislocation density.

We now impose the requirement that upon stress reversal, $\tau^\alpha \rightarrow -\tau^\alpha$, the strain rate is also reversed: $\dot{\gamma}^\alpha \rightarrow -\dot{\gamma}^\alpha$. (This requirement was not necessary in polycrystalline plasticity calculations where we used the von Mises stress \bar{s} , which is always non-negative, in place of the resolved shear stress τ^α ; see for example Lieou and Bronkhorst (2018).) Thus we subtract from Eq. (32) the term $f(-\tau^\alpha, \bar{\rho}^\alpha)$ to preserve symmetry:

$$\dot{\gamma}^\alpha = \frac{1}{t_0} [f(\tau^\alpha, \bar{\rho}^\alpha) - f(-\tau^\alpha, \bar{\rho}^\alpha)] \equiv \frac{g(\tau^\alpha, \bar{\rho}^\alpha)}{t_0}. \quad (33)$$

This is necessary to ensure that dislocation slip is strictly dissipative. Since structural evolution is driven by plastic work rate as given in Eqs. (21) and (22), it remains physically correct with load reversal. Additionally, following Langer et al. (2010) and Langer (2015), Eq. (32) for the slip rate allows us to compute the hardening parameter κ_ρ^α , by considering the onset of strain hardening, when the resolved shear stress is roughly equal to the Taylor stress s_T^α , but the dislocation density is still small. The conclusion is that κ_ρ^α can be written in the form

$$\kappa_\rho^\alpha = \frac{\kappa_1^\alpha}{(\bar{\nu}^\alpha)^2}, \quad (34)$$

where

$$\bar{\nu}^\alpha \equiv \ln\left(\frac{T_P}{T}\right) - \ln\left[\ln\left(\frac{\bar{\rho}^\alpha}{t_0|\dot{\gamma}_0^\alpha|\sqrt{\sum_\beta d^{\alpha\beta}\bar{\rho}^\beta}}\right)\right], \quad (35)$$

with

$$\dot{\gamma}_0^\alpha \equiv (\mathbf{F}^e)^{-1} \mathbf{L} \mathbf{F}^e : (\mathbf{s}^\alpha \otimes \mathbf{m}^\alpha) \quad (36)$$

being the total shear rate resolved in slip plane α .

3. Computational method

The thermodynamic theory of crystal plasticity outlined above was implemented in the implicit branch of Abaqus (Smith, 2014), following the numerical integration scheme outlined in Kalidindi et al. (1992) and Bronkhorst et al. (1992). We simulated a polycrystal fcc copper cube of lateral dimension 1 mm comprised of 1000 eight-node linear brick elements with full integration undergoing uniaxial compression, up to a true strain of unity. The simple computational model assumed each element was assigned an individual grain and periodic boundary conditions applied to the surfaces as in (Bronkhorst et al., 2007). The same polycrystal cube was also used for the simple shear and uniaxial tension simulations, to be described in Sec. 5.

The implicit finite-element method uses a Newton-type iteration scheme for computing estimates of the nodal displacement, which necessitates the computation of the Jacobian matrix

$$\mathcal{W} = \frac{\partial \bar{\boldsymbol{\sigma}}}{\partial \bar{\mathbf{e}}}, \quad (37)$$

where $\vec{\sigma}$ and \vec{e} are vector representations of the Cauchy stress tensor σ and symmetric relative strain tensor e , evaluated at time $t + \Delta t$ as follows:

$$\vec{\sigma} = \begin{bmatrix} \sigma_{11}(t + \Delta t) \\ \sigma_{22}(t + \Delta t) \\ \sigma_{33}(t + \Delta t) \\ \sigma_{12}(t + \Delta t) \\ \sigma_{13}(t + \Delta t) \\ \sigma_{23}(t + \Delta t) \end{bmatrix}; \quad \vec{e} = \begin{bmatrix} e_{11}(t + \Delta t) \\ e_{22}(t + \Delta t) \\ e_{33}(t + \Delta t) \\ e_{12}(t + \Delta t) \\ e_{13}(t + \Delta t) \\ e_{23}(t + \Delta t) \end{bmatrix}. \quad (38)$$

The relative strain tensor e is given by

$$e = \ln \mathbf{U}^t, \quad (39)$$

where \mathbf{U}^t is the relative stretch obtained from the polar decomposition of the relative deformation gradient \mathbf{F}^t :

$$\mathbf{F}(t + \Delta t) = \mathbf{F}^t \mathbf{F}(t); \quad \mathbf{F}^t = \mathbf{R}^t \mathbf{U}^t. \quad (40)$$

To compute the Jacobian in Eq. (37), note first the relationship between the Cauchy stress tensor $\sigma(t + \Delta t)$ and the second Piola-Kirchoff stress tensor $\mathbf{S}(t + \Delta t)$ at time $t + \Delta t$ are related by (c.f. Eq. (3) above)

$$\sigma(t + \Delta t) = \frac{1}{\det \mathbf{F}^e(t + \Delta t)} \mathbf{F}^e(t + \Delta t) \mathbf{S}(t + \Delta t) (\mathbf{F}^e)^T(t + \Delta t), \quad (41)$$

so that, upon taking infinitesimal variation and suppressing the argument $t + \Delta t$,

$$\delta \sigma = \frac{1}{\det \mathbf{F}^e} \left[\delta \mathbf{F}^e \mathbf{S} (\mathbf{F}^e)^T + \mathbf{F}^e \delta \mathbf{S} (\mathbf{F}^e)^T + \mathbf{F}^e \mathbf{S} \delta (\mathbf{F}^e)^T - (\mathbf{F}^e \mathbf{S} (\mathbf{F}^e)^T) \text{tr} (\delta \mathbf{F}^e (\mathbf{F}^e)^{-1}) \right]. \quad (42)$$

If we define the fourth-rank tensors \mathcal{T} and \mathcal{Q} as follows:

$$\mathcal{T} \equiv \frac{\partial \mathbf{F}^e}{\partial \mathbf{e}}; \quad \mathcal{Q} \equiv \frac{\partial \mathbf{S}}{\partial \mathbf{e}}, \quad (43)$$

then the fourth-rank representation of the Jacobian defined in Eq. (37) is given by

$$\delta \sigma_{ij} \equiv \mathcal{W}_{ijkl} \delta e_{kl}; \quad (44)$$

$$\mathcal{W}_{ijkl} = \frac{1}{\det \mathbf{F}^e} \left[\mathcal{T}_{imkl} S_{mn} F_{nj}^{eT} + F_{im}^e \mathcal{Q}_{mnkl} F_{nj}^{eT} + F_{im}^e S_{mn} \mathcal{T}_{j nkl} - F_{im}^e S_{mn} F_{nj}^{eT} (\mathcal{T}_{pqkl} F_{qp}^{e-1}) \right]. \quad (45)$$

This can be converted to the second-rank form in Eq. (37) by means of the transformation

$$\mathcal{W} = \begin{bmatrix} \mathcal{W}_{1111} & \mathcal{W}_{1122} & \mathcal{W}_{1133} & (\mathcal{W}_{1112} + \mathcal{W}_{1121})/2 & (\mathcal{W}_{1113} + \mathcal{W}_{1131})/2 & (\mathcal{W}_{1123} + \mathcal{W}_{1132})/2 \\ \mathcal{W}_{2211} & \mathcal{W}_{2222} & \mathcal{W}_{2233} & (\mathcal{W}_{2212} + \mathcal{W}_{2221})/2 & (\mathcal{W}_{2213} + \mathcal{W}_{2231})/2 & (\mathcal{W}_{2223} + \mathcal{W}_{2232})/2 \\ \mathcal{W}_{3311} & \mathcal{W}_{3322} & \mathcal{W}_{3333} & (\mathcal{W}_{3312} + \mathcal{W}_{3321})/2 & (\mathcal{W}_{3313} + \mathcal{W}_{3331})/2 & (\mathcal{W}_{3323} + \mathcal{W}_{3332})/2 \\ \mathcal{W}_{1211} & \mathcal{W}_{1222} & \mathcal{W}_{1233} & (\mathcal{W}_{1212} + \mathcal{W}_{1221})/2 & (\mathcal{W}_{1213} + \mathcal{W}_{1231})/2 & (\mathcal{W}_{1223} + \mathcal{W}_{1232})/2 \\ \mathcal{W}_{1311} & \mathcal{W}_{1322} & \mathcal{W}_{1333} & (\mathcal{W}_{1312} + \mathcal{W}_{1321})/2 & (\mathcal{W}_{1313} + \mathcal{W}_{1331})/2 & (\mathcal{W}_{1323} + \mathcal{W}_{1332})/2 \\ \mathcal{W}_{2311} & \mathcal{W}_{2322} & \mathcal{W}_{2333} & (\mathcal{W}_{2312} + \mathcal{W}_{2321})/2 & (\mathcal{W}_{2313} + \mathcal{W}_{2331})/2 & (\mathcal{W}_{2323} + \mathcal{W}_{2332})/2 \end{bmatrix}. \quad (46)$$

For small incremental stretch,

$$\mathbf{e} = \ln \mathbf{U}^t \approx \mathbf{U}^t - 1, \quad (47)$$

so that $\delta \mathbf{e} = \delta \mathbf{U}^t$, and hence

$$\mathcal{T} \approx \frac{\partial \mathbf{F}^e}{\partial \mathbf{U}^t}; \quad \mathcal{Q} \approx \frac{\partial \mathbf{S}}{\partial \mathbf{U}^t}. \quad (48)$$

It suffices to compute these two quantities in order to evaluate the Jacobian \mathcal{W} . We list the steps below without proof; readers interested in the derivation may consult, for example, Balasubramanian (1998).

1. Compute the fourth-rank matrix

$$\mathcal{L}_{ijkl} = F_{ik}^{e^T}(t) U_{lm}^t(t + \Delta t) F_{mj}^e(t) + F_{im}^{e^T}(t) U_{mk}^t(t + \Delta t) F_{ij}^e(t).$$

2. Let \mathcal{C}_{ijkl}^c denote the anisotropic elastic modulus tensor in the crystal basis, and let \mathbf{Q} denote the orthogonal rotation from the crystal basis to the global coordinates. Compute the anisotropic elastic modulus tensor in the global basis, \mathcal{C}_{ijkl} , as follows:

$$\mathcal{C}_{ijkl} = Q_{im} Q_{jn} Q_{kp} Q_{lq} \mathcal{C}_{mnpq}^c.$$

Use this result to calculate

$$\mathcal{D}_{ijkl} = \frac{1}{2} \mathcal{C}_{ijmn} \mathcal{L}_{mnkl}.$$

3. Let $\mathbf{N}^\alpha \equiv \mathbf{s}^\alpha \otimes \mathbf{m}^\alpha$ be the Schmid tensor for slip system α , in the reference configuration. For each α , compute

$$\begin{aligned} \mathcal{G}_{mnkl}^\alpha &= \mathcal{L}_{mpkl} N_{pn}^\alpha + N_{mp}^{\alpha^T} \mathcal{L}_{pnkl}; \\ \mathcal{J}_{ijkl}^\alpha &= \frac{1}{2} \mathcal{C}_{ijmn} \mathcal{G}_{mnkl}^\alpha. \end{aligned}$$

4. Compute the matrix

$$B_{ij}^\alpha = \frac{\Delta t}{2} \frac{\partial \dot{\gamma}^\alpha(t)}{\partial \tau^\alpha} (N_{ij}^\alpha + N_{ji}^\alpha).$$

5. Compute the fourth-rank matrices

$$\begin{aligned} \mathcal{K}_{ijkl} &= \mathcal{I}_{ijkl} + \sum_{\alpha} C_{ij}^\alpha B_{kl}^\alpha; \\ \mathcal{Q}_{ijkl} &= \mathcal{K}_{ijmn}^{-1} \left(\mathcal{D}_{mnkl} - \sum_{\alpha} \dot{\gamma}^\alpha \Delta t \mathcal{J}_{mnkl}^\alpha \right). \end{aligned}$$

In the first of these equations, \mathcal{I}_{ijkl} is the fourth-rank identity matrix.

6. Compute the quantities

$$\begin{aligned} R_{ij}^\alpha &= B_{kl}^\alpha \mathcal{Q}_{kl ij}; \\ \mathcal{T}_{ijkl} &= R_{ik}^t \left(F_{lj}^e(t) - F_{lp}^e(t) \sum_{\alpha} \dot{\gamma}^\alpha \Delta t N_{pj}^\alpha \right) - R_{im}^t U_{mn}^t F_{np}^e(t) \sum_{\alpha} R_{kl}^\alpha N_{pj}^\alpha. \end{aligned}$$

7. Finally, compute the Jacobian

$$\mathcal{W}_{ijkl} = \frac{1}{\det \mathbf{F}^e} \left[\mathcal{T}_{imkl} S_{mn} F_{nj}^{e^T} + F_{im}^e \mathcal{Q}_{mnkl} F_{nj}^{e^T} + F_{im}^e S_{mn} \mathcal{T}_{jnkl} - F_{im}^e S_{mn} F_{nj}^{e^T} (\mathcal{T}_{pqkl} F_{qp}^{e^{-1}}) \right].$$

4. Uniaxial compression of copper: model results

4.1. Parameter selection and evaluation

The uniaxial compression experimental results used for parameter evaluation in this work are those from Chen and Gray (2019) and Follansbee and Kocks (1988) where they present the stress-strain curves of OFHC copper at multiple conditions of strain rate and initial temperature.

The parameters used in our computation are listed in Table 2. Many of the material parameters for fcc copper, such as those that determine the elastic moduli and the heat capacity, are well known. In particular, we assume that the mass density $\bar{\rho}_M$ and specific heat capacity c_p to be constants for the loading conditions described in this manuscript, and stipulate that the crystallographic elastic moduli vary linearly with temperature:

$$C_{ij}(T) = C_{ij}^0 + m_{ij}T, \quad (49)$$

Table 2: List of parameters and initial conditions

Parameter	Definition or meaning	Value
$\bar{\rho}_M$	Mass density	8960 kg m ⁻³
c_p	Specific heat capacity	380 J kg ⁻¹ K ⁻¹
C_{11}^0	Elastic moduli parameter	179.5 GPa
m_{11}	Elastic moduli parameter	-36.3 MPa K ⁻¹
C_{12}^0	Elastic moduli parameter	126.4 GPa
m_{12}	Elastic moduli parameter	-16.4 MPa K ⁻¹
C_{44}^0	Elastic moduli parameter	82.5 GPa
m_{44}	Elastic moduli parameter	25.7 MPa K ⁻¹
μ_1	Shear modulus adjustment	6 GPa
α_T	Stress scale parameter	2
b	Burgers vector	0.257 nm
a^{self}	Dislocation interaction coefficient	0.122
a^{copl}	Dislocation interaction coefficient	0.122
a^{hirth}	Dislocation interaction coefficient	0.070
a^{colli}	Dislocation interaction coefficient	0.625
a^{gliss}	Dislocation interaction coefficient	0.137
a^{lomer}	Dislocation interaction coefficient	0.122
k_c	Mean free path parameter	12.0
k_{nc}	Mean free path parameter	180.0
a	Atomic length scale	5.14 nm
$(a/b)t_0$	Atomic time scale	1 ps
T_P	Depinning barrier	40800 K
χ_{ss}	Steady-state effective temperature (in units of e_D)	0.25
κ_1^α	Hardening parameter	100.0
κ_χ	Effective temperature increase rate	6.0

with $\{ij\} = \{11\}$, $\{12\}$, or $\{44\}$, which give the temperature-dependent single-crystal shear modulus according to the relationship

$$\mu_{\text{sc}}(T) = \sqrt{C_{44}(T) \left(\frac{C_{11}(T) - C_{12}(T)}{2} \right)}. \quad (50)$$

To account for the effect of grain boundaries on the shear stiffness, we empirically adjust the shear modulus of the polycrystal OFHC copper as follows:

$$\mu(T) = \mu_{\text{sc}}(T) + \mu_1, \quad (51)$$

where μ_1 is a constant for our purposes. This is consistent with typical hand-book and experimental data (e.g., Simmons and Wang, 1971) that indicates that the shear modulus of the polycrystal aggregate is uniformly higher than $\mu_{\text{sc}}(T)$ computed in accordance with Eq. (50), with some uncertainty.

In this work we suppose that the dislocation interaction coefficients $a^{\alpha\beta}$ and $d^{\alpha\beta}$, which determine the Taylor stress s_T^α and the dislocation mean

free path l^α respectively, are the same as in conventional literature (e.g., Kubin et al., 2008; Dequiedt et al., 2015; Bronkhorst et al., 2019). Specifically, in fcc copper, for which there are 12 slip systems and four slip planes, the set of quantities $a^{\alpha\beta}$ contains six independent coefficients as follows:

1. $a^{\alpha\alpha} = a^{\text{self}}$ (self interaction) ;
2. $a^{\alpha\beta} = a^{\text{copl}}$ if $\mathbf{m}^\alpha = \mathbf{m}^\beta$ and $\mathbf{s}^\alpha \neq \mathbf{s}^\beta$ (dipolar interaction) ;
3. $a^{\alpha\beta} = a^{\text{hirth}}$ if $\mathbf{m}^\alpha \neq \mathbf{m}^\beta$ and $\mathbf{s}^\alpha \perp \mathbf{s}^\beta$ (Hirth lock) ;
4. $a^{\alpha\beta} = a^{\text{colli}}$ if $\mathbf{m}^\alpha \neq \mathbf{m}^\beta$ and $\mathbf{s}^\alpha = \mathbf{s}^\beta$ (collinear interaction) ;
5. $a^{\alpha\beta} = a^{\text{gliss}}$ if $\mathbf{m}^\alpha \neq \mathbf{m}^\beta$, $\mathbf{s}^\alpha \neq \mathbf{s}^\beta$ with one of the two slip directions in both slip planes (glissile junction) ;
6. $a^{\alpha\beta} = a^{\text{lomer}}$ otherwise (Lomer lock) .

The mean free path coefficients are given by

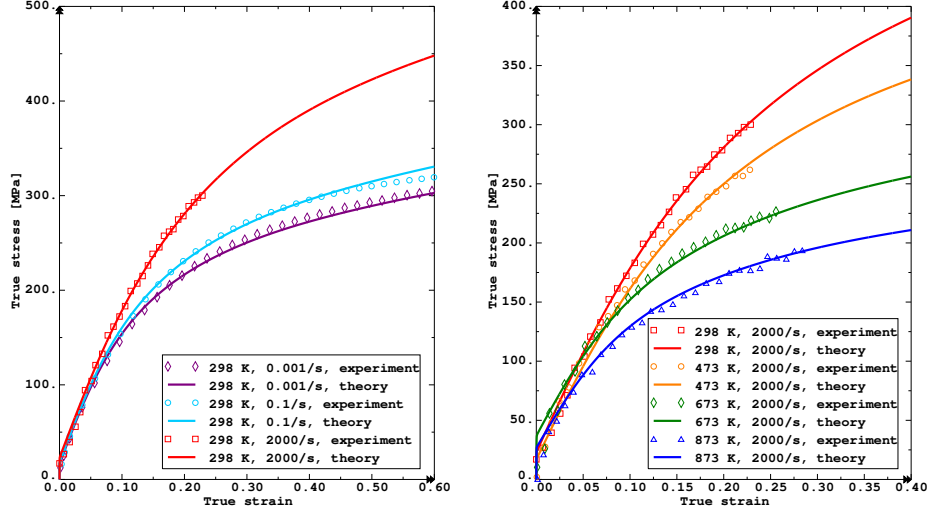
$$d^{\alpha\beta} = \frac{a^{\alpha\beta}}{k_c^2} \quad (52)$$

for intersecting slip systems, and

$$d^{\alpha\beta} = \frac{a^{\alpha\beta}}{k_{nc}^2} \quad (53)$$

for self interaction and coplanar slip systems. There is uncertainty in the values of k_c and k_{nc} but it appears from the present study to have a mostly cosmetic effect on the stress-strain curves.

Other parameters need to be determined separately. While Langer et al. (2010) and Langer (2015), in their work on the isotropic version of the thermodynamic dislocation theory for which there is only one single dislocation density variable, provided the values of many of these parameters, there is no a priori reason why values of parameters that pertain to dislocation generation and motion should remain unaltered in going from one dislocation density to 12 dislocation densities on as many distinct slip systems, which give rise to complex interactions between dislocations. Scalar thermodynamic parameters, however, should not depend on whether we adopt an isotropic or crystal-plasticity description. Thus, the dislocation depinning barrier T_P , which was unambiguously determined in Langer et al. (2010) to be around 40800 K from the steady-state stress of the experimental data available to them, should remain the same in our present calculations, even though we do not have the luxury of clean steady-state stresses at high temperatures



(a) $T = 298$ K, various loading rates (b) Various temperatures, 2000 s^{-1}

Figure 1: Stress-strain behavior of the millimeter-cube fcc copper polycrystal under uniaxial compression.

at our disposal. In the same spirit, the steady-state effective temperature χ_{ss} , in units of the dislocation formation energy e_D , is taken to be 0.25, as in the literature on the scalar, isotropic version of the TDT theory, since the effective temperature describes the state of inherent structural disorder. We then adjust κ_1^α to fit the initial hardening rate; the ratio a/b and the rate parameter κ_χ , the ratio of length scales a/b , and the initial effective temperature are adjusted to fit the data at large strains. Importantly, there is no a priori reason why the distinct samples tested at different thermal temperatures T must share the same initial dislocation densities and effective temperature. Importantly, the stress-strain behavior depends only on the product $(a/b)\alpha_T$ if the initial dislocation densities ρ^α adjusted accordingly, inversely proportional to the ratio a/b , with all other parameters and initial conditions held fixed. This freedom of parameter selection is addressed by choosing a/b , where a is the minimum separation between dislocation lines on a given slip system, to be of $\mathcal{O}(10)$, while using reasonable values for the initial dislocation densities.

Table 3: List of initial dislocation densities $\rho^\alpha(t = 0)$ and effective temperature $\chi(t = 0)$ for uniaxial compression

Temperature (K)	Strain rate (s^{-1})	$\rho^\alpha(t = 0)$ (mm^{-2})	$\chi(t = 0)$
298	0.001	2×10^5	0.185
298	0.1	2×10^5	0.185
298	2000	2×10^5	0.195
473	2000	2×10^6	0.21
673	2000	2×10^6	0.21
873	2000	2×10^6	0.225

4.2. Results

Simulations on the millimeter-cube fcc copper under uniaxial compression were performed, at a (true) strain rate of 10^{-3} s^{-1} and 10^{-1} s^{-1} for an initial temperature of $T(t = 0) = 298 \text{ K}$, and at a strain rates of $2 \times 10^3 \text{ s}^{-1}$ for temperatures $T(t = 0) = 298, 473, 673$, and 873 K . We assume isothermal deformation; the adiabatic assumption at the highest strain rate does not result in appreciable difference in the stress-strain response, in the strain regime for which experimental data is available to us. In other words, there is insufficient information for us to determine whether deformation is isothermal or adiabatic, or the value of the Taylor-Quinney coefficient. The initial conditions are listed in Table 3; grain orientations are determined from EBSD data. The results are shown in Fig. 1, demonstrating good agreement between theory and experiment.

5. Uniaxial tension and simple shear

To further validate the thermodynamic dislocation theory, we perform finite-element simulations, using the procedure described in Sec. 3, on the same polycrystal cube subjected to uniaxial tension and simple shear; we compare its stress-strain behavior with experiments described in Bronkhorst et al. (1992). The results are shown in Figs. 2 and 3 and demonstrate good agreement. There was no need for us to adjust any of the material parameters listed in Table 2. However, we had to slightly adjust the initial dislocation densities and effective temperatures, as described in Table 4, in order to arrive at agreement at intermediate strains. This is not surprising. There is no reason a priori that material preparation for the Bronkhorst et al. (1992) experiments would result in the same dislocation densities, grain size, grain orientations, and state of configurational disorder, as in Follansbee and Kocks

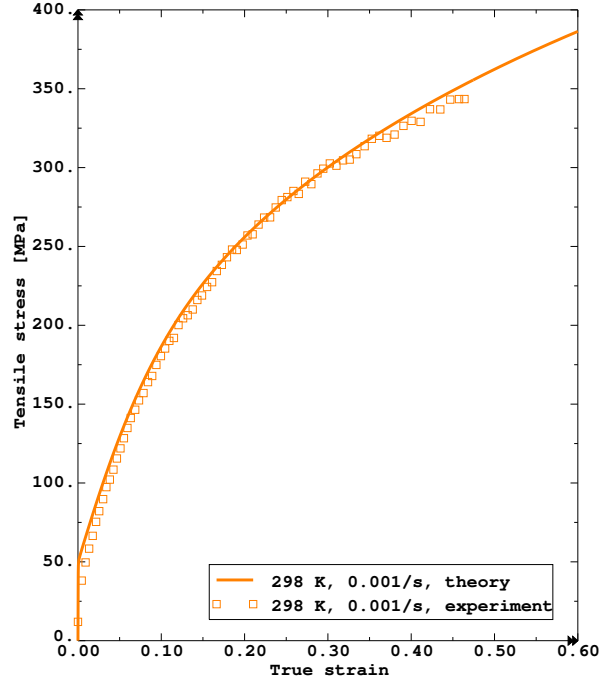


Figure 2: Stress-strain curve for the copper polycrystal undergoing uniaxial tension, at a true strain rate of 10^{-3} s^{-1} and temperature $T = 298 \text{ K}$.

(1988) and Chen and Gray (2019); yet these initial conditions do influence the stress-strain response. That being said, both the initial hardening rate and the hardening rate at intermediate strains depend only on the material parameters in Table 2 and not on material preparation; thus the present agreement between theory and experiments provides a strong validation of the thermodynamic dislocation theory.

6. Discussions

The thermodynamic dislocation theory described here is based on the premise that dislocations in a deforming crystal constitute material configurations that can, in principle, be enumerated. Thus, a system of dislocations correspond to some configurational energy and entropy and, therefore, a well-defined configurational or effective temperature. This effective temperature is ordinarily substantially higher than the thermal temperature, because

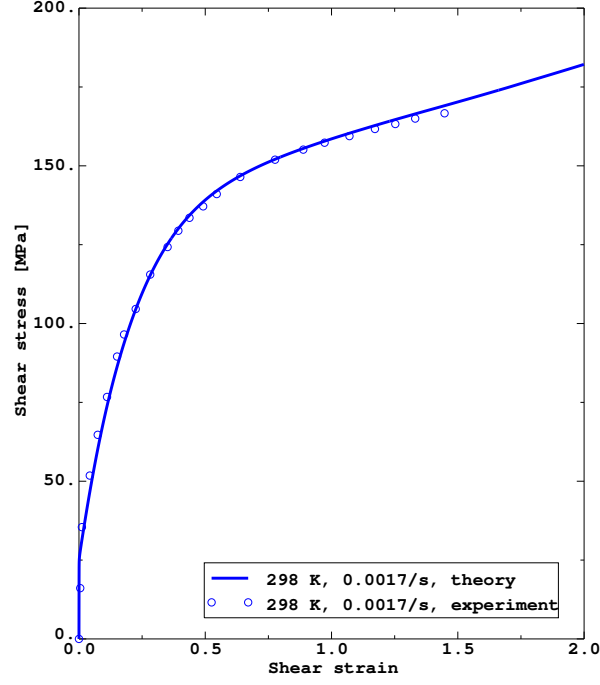


Figure 3: Stress-strain curve for the copper polycrystal undergoing simple shear, at a strain rate of $1.7 \times 10^{-3} \text{ s}^{-1}$ and temperature $T = 298 \text{ K}$.

Table 4: List of initial dislocation densities $\rho^\alpha(t = 0)$ and effective temperature $\chi(t = 0)$ for uniaxial tension and simple shear

Experiment	Temperature (K)	Strain rate (s^{-1})	$\rho^\alpha(t = 0)$ (mm^{-2})	$\chi(t = 0)$
Uniaxial tension	298	0.001	2×10^6	0.19
Simple shear	298	0.0017	2×10^6	0.18

thermal fluctuations alone can affect dislocation mobility but the energy represented is not great enough to create dislocations during deformation. This is then the foundation of thermally activated dislocation motion where motion is still dominated by plastic work put into the material. As a result, the configurational subsystem of the deforming crystal is only weakly coupled to the thermal subsystem, and is amenable to a thermodynamic description as described in this paper.

Our thermodynamic description contains two crucial ingredients. The first of these is the direct connection between the dislocation densities ρ^α in the non-equilibrium steady state and the effective temperature χ , as in Eq. (30); this is a consequence of the second law of thermodynamics, as is discussed earlier in the manuscript. The second crucial ingredient is the proportionality between the rate at which the dislocation densities evolve and the plastic work rate, as described by Eq. (21). This arises from the storage of input work in dislocation structures, and is an ingredient absent from most conventional continuum dislocation theories which are based largely on kinematics of dislocation motion only. These two physical ingredients constitute the most important elements of the TDT and make the theory thermodynamically consistent and also allow for inclusion of definitions of the Taylor-Quinney coefficient (Eq. (23)) which then become inherently related to the complete balance of energy within the system. The current model has been used to compute the evolution of the Taylor-Quinney coefficient for the different loading and state conditions covered in this work and is given in Fig. 4. As demonstrated the current theory illustrates an evolving value and differing slightly with loading rate. Recent experimental work also suggests that the value of this plastic power conversion factor is significantly less than 1.0 (Rittel et al., 2012, 2017; Kingstedt and Lloyd, 2019). Much more experimental work and parallel theoretical comparison with the experimental datasets is required to elucidate the evolution of material temperature with deformation. This will greatly facilitate our development of theories accounting for the energetics of dislocation motion and enable a path to understanding material damage under adverse loading conditions.

In going from the isotropic version of TDT (Langer et al., 2010; Langer, 2015) to the crystal-plasticity version, we encounter a number of important questions that pertain to the crystalline, non-isotropic nature of the solid. The first of these is that with as many dislocation density variables ρ^α as the number of slip systems, can we quantify the interaction between different slip systems? For fcc copper, we have been able to fit experimental data

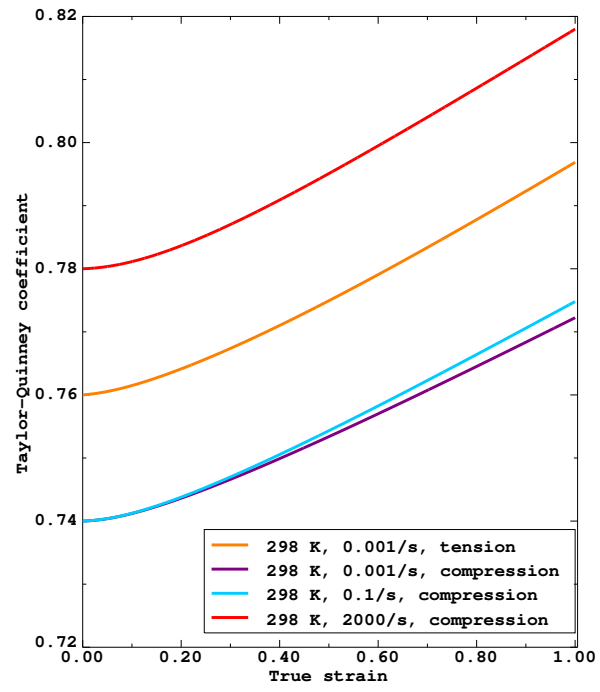


Figure 4: Computed value of the Taylor-Quinney coefficient as a function of strain for tension and compression modes of loading at room temperature and varying rates of deformation.

by assuming, as in conventional dislocation theories, prescribed slip resistances and mean free paths that couple the different slip systems (Eqs. (27), (52), and (53)), and set the interaction energy e_N between different slip systems to be equal to zero in Eq. (30), which in effect rules out latent hardening for the current study. As discussed within the introduction, this remains a very important area of research, to understand and quantify the nature of dislocation interactions and their observed formation of intragranular dislocation substructures as the physical root of observed material hardening. This dislocation structure evolution has important implications for material damage as the heterogeneous stress field will evolve with deformation. The theory proposed here as well as other recent work (Dequiedt et al., 2015; Grilli et al., 2018; Arora and Acharya, 2019) offer continuum representation of discrete dislocation processes which are however able to access comparisons with large experimental databases for many different material types. Advances to these continuum theories have already benefited from discrete dislocation dynamics simulations (e.g. (Madec et al., 2002, 2003; Devincre et al., 2006, 2008)) to quantify the differing interactions within the fcc crystal structure. This relationship between available experimental information, physics simulations of dislocation mechanics, and continuum theories is integral to making tangible progress. Although discrete dislocation dynamics generally lacks accounting for thermodynamic quantities, it is continuing to be used effectively for the study of dislocation mechanics (Rao et al., 2019; Cho et al., 2018; Santos-Guemes et al., 2018). New high-resolution continuum and phase field techniques hold promise for computing dislocation interaction kinetics with some able to do so in a thermodynamically consistent way (Acharya et al., 2004; Acharya and Roy, 2006; Acharya, 2010; Peng et al., 2020; Eghtesad et al., 2018; Arora and Acharya, 2019; Zeng et al., 2016). The modeling community is most advanced for fcc systems with significant amounts of work remaining to quantify slip for other common bcc and hcp crystal systems given that these systems are generally more complex.

7. Concluding remarks

In this paper, we formulated a single crystal, finite-deformation version of the thermodynamic dislocation theory, first pioneered by Langer, Bouchbinder, and Lookman (Langer et al., 2010; Langer, 2015) in the language of isotropic plasticity and infinitesimal deformation. With only a small handful

of adjustable parameters, finite-element simulations demonstrate favorable agreement between theory and a series of experiments on polycrystal fcc copper strained under a range of temperatures, loading rates, and loading configurations including uniaxial compression, tension, and simple shear. Our work constitutes an essential first step of this line of thought towards a physics-based, thermodynamically-consistent description of dislocation plasticity in arbitrary geometries and loading configurations. The topic of hardening and complex dislocation interactions represented via a continuum theory is introduced into this thermodynamic framework. The introduction of plastic work as an energy driver for the production of additional defects introduces the concept of the energy of interactions and the potential of interacting stress fields around the cores of dislocations as a factor in material hardening which will be explored further.

Acknowledgements

CL would like to thank J. S. Langer, K. C. Le, and R. A. Lebensohn for insightful discussions. CL was partially supported by the Center for Nonlinear Studies at the Los Alamos National Laboratory over the duration of this work. CB acknowledges support from the University of Wisconsin Alumni Research Foundation. All authors were partially supported by the DOE/DOD Joint Munitions Program and LANL LDRD Program Project 20170033DR. The authors declare no conflicts of interest.

References

References

- Acharya, A., 2010. New inroads in an old subject: plasticity, from around the atomic to the macroscopic scale. *Journal of the Mechanics and Physics of Solids* 58 (5), 766–778.
- Acharya, A., Roy, A., 2006. Size effects and idealized dislocation microstructure at small scales: Predictions of a phenomenological model of mesoscopic field dislocation mechanics: Part i. *J. Mech. Phys. Solids* 54, 1687–1710.
- Acharya, A., Tang, H., Saigal, S., Bassani, J. L., 2004. On boundary conditions and plastic strain-gradient discontinuity in lower-order gradient plasticity. *J. Mech. Phys. Solids* 52, 1793–1826.

- Aifantis, E. C., 1992. On the role of gradients in the localization of deformation and fracture. *Int. J. Eng. Sci.* 30 (10), 1279–1299.
- Anand, L., Gurtin, M. E., Lele, S. P., Gething, C., 2005. A one-dimensional theory of strain-gradient plasticity: Formulation, analysis, numerical results. *J. Mech. Phys. Solids* 53, 1789–1826.
- Anand, L., Gurtin, M. E., Reddy, B. D., 2015. The stored energy of cold work, thermal annealing, and other thermodynamic issues in single crystal plasticity at small length scales. *International Journal of Plasticity* 64, 1 – 25.
URL <http://www.sciencedirect.com/science/article/pii/S074964191400148X>
- Arora, R., Acharya, A., 2019. Dislocation pattern formation in finite deformation crystal plasticity. *Int. J. Solids Struct.* in press.
- Arsenlis, A., Parks, D. M., 1999. Crystallographic aspects of geometrically-necessary and statistically-stored dislocation density. *Acta mater.* 47 (5), 1597–1611.
- Arsenlis, A., Parks, D. M., 2002. Modeling the evolution of crystallographic dislocation density in crystal plasticity. *J. Mech. Phys. Solids* 50, 1979–2009.
- Asaro, R., Rice, J., 1977. Strain localization in ductile single crystals. *Journal of the Mechanics and Physics of Solids* 25 (5), 309 – 338.
URL <http://www.sciencedirect.com/science/article/pii/0022509677900011>
- Asaro, R. J., 1983a. Crystal plasticity. *J. Appl. Mech.* 50, 921–934.
- Asaro, R. J., 1983b. Micromechanics of crystals and polycrystals. *Adv. Appl. Mech.* 23, 1–115.
- Asaro, R. J., Needleman, A., 1985. Texture development and strain hardening in rate dependent polycrystals. *Acta metall.* 33, 923–953.
- Balasubramanian, S., 2 1998. Polycrystalline plasticity: application to deformation processing of lightweight metals. Ph.D. thesis, Massachusetts Institute of Technology, Cambridge, MA.

- Barton, N. R., Benson, D. J., Becker, R., jun 2005. Crystal level continuum modelling of phase transformations: the $\alpha \leftrightarrow \epsilon$ transformation in iron. *Modelling and Simulation in Materials Science and Engineering* 13 (5), 707–731.
- Bassani, J. L., 1993. Plastic flow of crystals. *Adv. Appl. Mech.* 30, 191–258.
- Bassani, J. L., Wu, T.-Y., 1991. Latent hardening in single crystals. ii. analytical characterization and predictions. *Proc. Roy. Soc. Lond. A* 435, 21–41.
- Benzerga, A., Brchet, Y., Needleman, A., der Giessen, E. V., 2005. The stored energy of cold work: Predictions from discrete dislocation plasticity. *Acta Materialia* 53 (18), 4765 – 4779.
URL <http://www.sciencedirect.com/science/article/pii/S1359645405003964>
- Berdichevsky, V., 2018a. Why is classical thermodynamics insufficient for solids?
URL <https://arc.aiaa.org/doi/abs/10.2514/6.2018-0696>
- Berdichevsky, V. L., 2006. On thermodynamics of crystal plasticity. *Scripta Materialia* 54, 711–716.
- Berdichevsky, V. L., 2017. A continuum theory of edge dislocations. *J. Mech. Phys. Solids* 106, 95–132.
- Berdichevsky, V. L., 2018b. Entropy and temperature of microstructure in crystal plasticity. *Int. J. Eng. Science* 128, 24–30.
- Berdichevsky, V. L., 2019a. Beyond classical thermodynamics: Dislocation-mediated plasticity. *J. Mech. Phys. Solids* 129, 83–118.
- Berdichevsky, V. L., 2019b. Dynamic equations for a periodic set of edge dislocations. *Arch. Appl. Mech.* 89, 425–436.
- Boyce, B., Kramer, S., Bosiljevac, T., Corona, E., Moore, J., K. Elkhodary, C. S., Williams, B., Cerrone, A., Nonn, A., Hochhalter, J., Bomarito, G., Warner, J., Carter, B., Warner, D., Ingraffea, A., Zhang, T., Fang, X., Lua, J., Chiaruttini, V., Mazire, M., Feld-Payet, S., Yastrebov, V., Besson, J., Chaboche, J.-L., Lian, J., Di, Y., Wu, B., Novokshanov, D., Vajragupta, N., Kucharczyk, P., Brinnel, V., Dbereiner, B., Mnstermann,

- S., Neilsen, M., Dion, K., Karlson, K., Foulk, J., Brown, A., Veilleux, M., Bignell, J., Sanborn, S., Jones, C., Mattie, P., Pack, K., Wierzbicki, T., Chi, S.-W., Lin, S.-P., Mahdavi, A., Predan, J., Zadravec, J., Gross, A., Ravi-Chandar, K., Xue, L., 2016. The second sandia fracture challenge predictions of ductile failure under quasi-static and moderate-rate dynamic loading. *Int. J. Fract.* 198, 5–100.
- Boyce, B. L., Kramer, S. L. B., Fang, H. E., Cordova, T. E., Neilsen, M. K., Dion, K., Kaczmarowski, A. K., Karasz, E., Xue, L., Gross, A. J., Ghahremaninezhad, A., Ravi-Chandar, K., Lin, S.-P., Chi, S.-W., Chen, J. S., Yreux, E., Ruter, M., Qian, D., Zhou, Z., Bhamare, S., O'Connor, D. T., Tang, S., Elkhodary, K. L., Zhao, J., Hochhalter, J. D., Cerrone, A. R., Ingraffea, A. R., Wawrzynek, P. A., Carter, B. J., Emery, J. M., Veilleux, M. G., Yang, P., Gan, Y., Zhang, X., Chen, Z., Madenci, E., Kilic, B., Zhang, T., Fang, E., Liu, P., Lua, J., Nahshon, K., Miraglia, M., Cruce, J., DeFrese, R., Moyer, E. T., Brinckmann, S., Quinkert, L., Pack, K., Luo, M., Wierzbicki, T., 2014. The sandia fracture challenge: blind round robin predictions of ductile tearing. *Int. J. Fract.* 186, 5–68.
- Bronkhorst, C., Hansen, B., Cerreta, E., Bingert, J., 2007. Modeling the microstructural evolution of metallic polycrystalline materials under localization conditions. *Journal of the Mechanics and Physics of Solids* 55 (11), 2351 – 2383.
URL <http://www.sciencedirect.com/science/article/pii/S0022509607000804>
- Bronkhorst, C., Mayeur, J., Livescu, V., Pokharel, R., Brown, D., Gray, G., 2019. Structural representation of additively manufactured 316l austenitic stainless steel. *International Journal of Plasticity*.
URL <http://www.sciencedirect.com/science/article/pii/S0749641918307654>
- Bronkhorst, C. A., III, G. T. G., Addessio, F. L., Livescu, V., Bourne, N. K., McDonald, S. A., Withers, P. J., 2016. Response and representation of ductile damage under varying shock loading conditions in tantalum. *Journal of Applied Physics* 119.
- Bronkhorst, C. A., Kalidindi, S. R., Anand, L., 1992. Polycrystalline plasticity and the evolution of crystallographic texture in fcc metals. *Philosophical Transactions of the Royal Society of London. Series A: Physical and Engineering Sciences* 341 (1662), 443–477.
URL <https://royalsocietypublishing.org/doi/abs/10.1098/rsta.1992.0111>

- Brown, D. W., Adams, D. P., Balogh, L., Carpenter, J. S., Clausen, B., King, G., Reedlunn, B., Palmer, T. A., Maguire, M. C., Vogel, S. C., 2017. In situ neutron diffraction study of the influence of microstructure on the mechanical response of additively manufactured 304l stainless steel. *Metallurgical and Materials Transactions A* 48 (Dec), 6055–6069.
- Bulatov, V. V., Cai, W., 2007. *Computer Simulations of Dislocations*. Oxford University Press.
- Bunge, H. J., 1982. *Texture Analysis in Materials Science*. Butterworth.
- Busso, E. P., McClintock, F. A., 1996. A dislocation mechanics-based crystallographic model of a b2-type intermetallic alloy. *Int. J. Plasticity* 12 (1), 1–28.
- Busso, E. P., Meissonnier, F. T., O’Dowd, N. P., 2000. Gradient-dependent deformation of two-phase single crystals. *J. Mech. Phys. Solids* 48, 2333–2361.
- Chen, S. R., Gray, G. T., 2019. personal communication.
- Cheong, K.-S., Busso, E. P., 2004. Discrete dislocation density modelling of single phase fcc polycrystal aggregates. *Acta Materialia* 52 (19), 5665 – 5675.
URL <http://www.sciencedirect.com/science/article/pii/S1359645404005099>
- Cho, J., Molinari, J.-F., Curtin, W., Anciaux, G., 2018. The coupled atomistic/discrete-dislocation method in 3d. part iii: Dynamics of hybrid dislocations. *Journal of the Mechanics and Physics of Solids* 118, 1–14.
- Chowdhury, S. R., Roy, D., 2019. A non-equilibrium thermodynamic model for viscoplasticity and damage: Two temperatures and a generalized fluctuation relation. *Int. J. Plasticity* 113, 158–184.
- Clayton, J. D., 2011. *Nonlinear Mechanics of Crystals*. Springer.
- Coleman, B. D., Noll, W., Dec 1963. The thermodynamics of elastic materials with heat conduction and viscosity. *Archive for Rational Mechanics and Analysis* 13 (1), 167–178.
URL <https://doi.org/10.1007/BF01262690>

- del Castillo, P. E. J. R.-D., Huang, M., 2012. Dislocation annihilation in plastic deformation: I. multiscale irreversible thermodynamics. *Acta Materialia* 60, 2606–2614.
- Dequiedt, J., Denoual, C., Madec, R., 2015. Heterogeneous deformation in ductile fcc single crystals in biaxial stretching: the influence of slip system interactions. *Journal of the Mechanics and Physics of Solids* 83, 301 – 318.
URL <http://www.sciencedirect.com/science/article/pii/S0022509615001313>
- Devincre, B., Hoc, T., Kubin, L. P., 2008. Dislocation mean free paths and strain hardening of crystals. *Science* 320, 1745–1748.
- Devincre, B., Kubin, L. P., Hoc, T., 2006. Physical analysis of crystal plasticity by dd simulations. *Scripta Mater.* 54, 741–746.
- Duffy, J., Chi, Y., 1992. On the measurement of local strain and temperature during the formation of adiabatic shear bands. *Materials Science and Engineering: A* 157 (2), 195 – 210.
URL <http://www.sciencedirect.com/science/article/pii/092150939290026W>
- Eghtesad, A., Germaschewski, K., Beyerlein, I., Hunter, A., Knezevic, M., 2018. Graphics processing unit accelerated phase field dislocation dynamics: Application to bi-metallic interfaces. *Advances in Engineering Software* 115.
- Farren, W. S., Taylor, G. I., 1925. The heat developed during plastic extension of metals. *Proceedings of the Royal Society of London A: Mathematical, Physical and Engineering Sciences* 107 (743), 422–451.
URL <http://rspa.royalsocietypublishing.org/content/107/743/422>
- Feng, B., Bronkhorst, C., 2019. Three-dimensional modeling and simulations of single-crystal and bi-crystal titanium for high-strain-rate loading conditions. *International Journal of Plasticity* submitted.
- Feng, B., Bronkhorst, C. A., Addessio, F. L., Morrow, B. M., Li, W. H., Lookman, T., Cerreta, E. K., 2019. Coupled nonlinear elasticity, plastic slip, twinning, and phase transformation in single crystal titanium for plate impact loading. *J. Mech. Phys. Solids* 127, 358–385.
- Fleck, N. A., Hutchinson, J. W., 1993. A phenomenological theory for strain gradient effects in plasticity. *J. Mech. Phys. Solids* 41 (12), 1825–1857.

- Fleck, N. A., Hutchinson, J. W., 1997. Strain gradient plasticity. *Adv. Appl. Mech.* 33, 295–361.
- Follansbee, P. S., Kocks, U. F., 1988. A constitutive description of the deformation of copper based on the use of the mechanical threshold stress as an internal state variable. *Acta metall.* 36 (1), 81–93.
- Gerken, J. M., Dawson, P. R., 2008. A crystal plasticity model that incorporates stresses and strains due to slip gradients. *J. Mech. Phys. Solids* 56, 1651–1672.
- Gigax, J., Baldwin, J., Sheehan, C., Maloy, S., Li, N., 2019. Microscale shear specimens for evaluating the shear deformation in single-crystal and nanocrystalline cu and at cu-si interfaces. *Journal of Materials Research* 34 (9), 1574–1583.
- Grilli, N., Janssens, K. G. F., Nellessen, J., Sandlobes, S., Raabe, D., 2018. Multiple slip dislocation patterning in a dislocation-based crystal plasticity finite element method. *Int. J. Plasticity* 100, 104–121.
- Gurtin, M. E., 2000. On the plasticity of single crystals: free energy, microforces, plastic-strain gradients. *J. Mech. Phys. Solids* 48, 989–1036.
- Gurtin, M. E., Fried, E., Anand, L., 2010. *The Mechanics and Thermodynamics of Continua*. Cambridge University Press.
- Gurtin, M. E., Needleman, A., 2005. Boundary conditions in small-deformation, single-crystal plasticity that account for the burgers vector. *J. Mech. Phys. Solids* 53, 1–31.
- Hansen, B., Beyerlein, I., Bronkhorst, C., Cerreta, E., Dennis-Koller, D., 2013. A dislocation-based multi-rate single crystal plasticity model. *International Journal of Plasticity* 44, 129 – 146.
URL <http://www.sciencedirect.com/science/article/pii/S0749641912001957>
- Hansen, B. L., Bronkhorst, C. A., Ortiz, M., 2010. Dislocation sugrain structures and modeling the plastic hardening of metallic single crystals. *Mod. Sim. Mater. Sci. Eng.* 18, 055001.
- Harren, S. V., Asaro, R. J., 1989. Nonuniform deformations in polycrystals and aspets of the validity of the taylor model. *J. Mech. Phys. Solids* 37, 191–232.

- Harren, S. V., Lowe, T. C., Asaro, R. J., Needleman, A., 1989. Analysis of large-strain shear in rate-dependent face-centred cubic polycrystals: correlations of micro- and macromechanics. *Phil. Trans. R. Soc. Lond. A* 328, 443–500.
- Hartley, K., Duffy, J., Hawley, R., 1987. Measurement of the temperature profile during shear band formation in steels deforming at high strain rates. *Journal of the Mechanics and Physics of Solids* 35 (3), 283 – 301.
URL <http://www.sciencedirect.com/science/article/pii/0022509687900093>
- Hill, R., Rice, J. R., 1972. Constitutive analysis of elastic-plastic crystals at arbitrary strain. *J. Mech. Phys. Solids* 20, 401–413.
- Hochrainer, T., 2016. Thermodynamically consistent continuum dislocation dynamics. *J. Mech. Phys. Solids* 88, 12–22.
- Houtte, P. V., 1982. On the equivalence of the relaxed taylor theory and the bishop-hill theory for partially constrained plastic deformation of crystals. *Mater. Sci. Eng.* 55, 69–77.
- Houtte, P. V., 1988. A comprehensive mathematical formulation of an extended taylor-bishop-hill model featuring relaxed constraints, the renouard-wintenberger theory and a strain rate sensitivity model. *Textures Microstruct.* 8-9, 313–350.
- Houtte, P. V., Li, S., Seefeldt, M., Delannay, L., 2005. Deformation texture prediction from the taylor model to the advanced lamel model. *Int. J. Plasticity* 21, 589–624.
- Jafari, M., Jamshidian, M., Ziaei-Rad, S., 2017. A finite-deformation dislocation density-based crystal viscoplasticity constitutive model for calculating the stored deformation energy. *Int. J. Mech. Sciences* 128-129, 486–498.
- Jiang, M., Devincre, B., Monnet, G., 2019. Effects of the grain size and shape on the flow stress: A dislocation dynamics study. *Int. J. Plasticity* 113, 111–124.
- Kalidindi, S., Bronkhorst, C., Anand, L., 1992. Crystallographic texture evolution in bulk deformation processing of fcc metals. *Journal of the Mechanics and Physics of Solids* 40 (3), 537 – 569.
URL <http://www.sciencedirect.com/science/article/pii/0022509692800039>

- Kingstedt, O. T., Lloyd, J. T., 2019. On the conversion of plastic work to heat in mg alloy az31b for dislocation slip and twinning deformation. *Mechanics of Materials* 134, 176–184.
- Knezevic, M., Beyerlein, I. J., 2018. Multiscale modeling of microstructure-property relationships of polycrystalline metals during thermo-mechanical deformation. *Advanced Engineering Materials* 20 (4), 1700956.
URL <https://onlinelibrary.wiley.com/doi/abs/10.1002/adem.201700956>
- Kocks, U., Stout, M., Rollett, A., 1989. The influence of texture on strain hardeningwork supported by the u.s. department of energy, basic energy sciences. In: KETTUNEN, P., LEPIST, T., LEHTONEN, M. (Eds.), *Strength of Metals and Alloys (ICSMA 8)*. Pergamon, Oxford, pp. 25 – 34.
URL <http://www.sciencedirect.com/science/article/pii/B9780080348049500085>
- Kroner, E., 1960. Allgemeine kontinuumstheorie der versetzungen und eigenspannungen. *Archive for Rational Mechanics and Analysis* 4, 273–334.
- Kubin, L., Devincre, B., Hoc, T., 2008. Modeling dislocation storage rates and mean free paths in face-centered cubic crystals. *Acta Materialia* 56 (20), 6040 – 6049.
URL <http://www.sciencedirect.com/science/article/pii/S1359645408005788>
- Kubin, L. P., 2013. *Dislocations, mesoscale simulations and plastic flow*. Oxford University Press.
- Langer, J., Bouchbinder, E., Lookman, T., 2010. Thermodynamic theory of dislocation-mediated plasticity. *Acta Materialia* 58 (10), 3718 – 3732.
URL <http://www.sciencedirect.com/science/article/pii/S1359645410001540>
- Langer, J. S., Sep 2015. Statistical thermodynamics of strain hardening in polycrystalline solids. *Phys. Rev. E* 92, 032125.
URL <https://link.aps.org/doi/10.1103/PhysRevE.92.032125>
- Langer, J. S., Dec 2016. Thermal effects in dislocation theory. *Phys. Rev. E* 94, 063004.
URL <https://link.aps.org/doi/10.1103/PhysRevE.94.063004>

- Langer, J. S., Jan 2017a. Thermal effects in dislocation theory. ii. shear banding. *Phys. Rev. E* 95, 013004.
URL <https://link.aps.org/doi/10.1103/PhysRevE.95.013004>
- Langer, J. S., Mar 2017b. Yielding transitions and grain-size effects in dislocation theory. *Phys. Rev. E* 95, 033004.
URL <https://link.aps.org/doi/10.1103/PhysRevE.95.033004>
- Le, K., Tran, T., Langer, J., 2018. Thermodynamic dislocation theory of adiabatic shear banding in steel. *Scripta Materialia* 149, 62 – 65.
URL <http://www.sciencedirect.com/science/article/pii/S1359646218300836>
- Le, K. C., 2018. Thermodynamic dislocation theory for non-uniform plastic deformations. *J. Mech. Phys. Solids* 111, 157–169.
- Le, K. C., 2019. Thermodynamic dislocation theory: Finite deformations. *Int. J. Eng. Science* 139, 1–10.
- Lebensohn, R. A., 2001. N-site modeling of a 3d viscoplastic polycrystal using fast fourier transform. *Acta Materialia* 49, 2723–2737.
- Lebensohn, R. A., Tome, C. N., 1993. A self-consistent anisotropic approach for the simulation of plastic deformation and texture development of polycrystals: application to zirconium alloys. *Acta Metall. Mater.* 41, 2611–2624.
- Levitas, V. I., Javanbakht, M., 2015a. Interaction between phase transformations and dislocations at the nanoscale. part i. general phase field approach. *J. Mech. Phys. Solids* 82, 287–319.
- Levitas, V. I., Javanbakht, M., 2015b. Thermodynamically consistent phase field approach to dislocation evolution at small and large strains. *J. Mech. Phys. Solids* 82, 345–366.
- Levitas, V. I., Ma, Y. Z., Hashemi, J., Holtz, M., Guven, N., 2006. Strain-induced disorder, phase transformations, and transformation-induced plasticity in hexagonal boron nitride under compression and shear in a rotational diamond anvil cell: in situ x-ray diffraction study and modeling. *J. Chem. Phys.* 125, 044507.

- Lieou, C. K., Bronkhorst, C. A., 2018. Dynamic recrystallization in adiabatic shear banding: Effective-temperature model and comparison to experiments in ultrafine-grained titanium. *International Journal of Plasticity* 111, 107 – 121.
URL <http://www.sciencedirect.com/science/article/pii/S0749641918302821>
- Lieou, C. K., Mourad, H. M., Bronkhorst, C. A., 2019. Strain localization and dynamic recrystallization in polycrystalline metals: thermodynamic theory and simulation framework. *International Journal of Plasticity*.
- Longère, P., Dragon, A., 2008a. Evaluation of the inelastic heat fraction in the context of microstructure-supported dynamic plasticity modelling. *International Journal of Impact Engineering* 35 (9), 992 – 999.
URL <http://www.sciencedirect.com/science/article/pii/S0734743X07001054>
- Longère, P., Dragon, A., 2008b. Plastic work induced heating evaluation under dynamic conditions: Critical assessment. *Mechanics Research Communications* 35 (3), 135 – 141.
URL <http://www.sciencedirect.com/science/article/pii/S0093641307000894>
- Luscher, D. J., Buechler, M. A., Walters, D. J., Bolme, C., Ramos, K. J., 2018. On computing the evolution of temperature for materials under dynamic loading. *International Journal of Plasticity*.
URL <http://www.sciencedirect.com/science/article/pii/S0749641918301426>
- Madec, R., Devincre, B., Kubin, L. P., 2002. From dislocation junctions to forest hardening. *Phys. Rev. Lett.* 89, 255508.
- Madec, R., Devincre, B., Kubin, L. P., Hoc, T., Rodney, D., 2003. The role of collinear interaction in dislocation-induced hardening. *Science* 301, 1879–1882.
- Marchand, A., Duffy, J., 1988. An experimental study of the formation process of adiabatic shear bands in a structural steel. *Journal of the Mechanics and Physics of Solids* 36 (3), 251 – 283.
URL <http://www.sciencedirect.com/science/article/pii/0022509688900129>
- Mayeur, J., McDowell, D., 2015. Micropolar crystal plasticity simulation of particle strengthening. *Modelling and Simulation in Materials Science and Engineering* 23, 065007.

- Mayeur, J., McDowell, D., Bammann, D., 2011. Dislocation-based micropolar single crystal plasticity: Comparison of multi- and single criterion theories. *Journal of the Mechanics and Physics of Solids* 59, 398–422.
- Mecking, H., Kocks, U., 1981. Kinetics of flow and strain-hardening. *Acta Metallurgica* 29 (11), 1865 – 1875.
URL <http://www.sciencedirect.com/science/article/pii/0001616081901127>
- Mourad, H., Bronkhorst, C., Livescu, V., Plohr, J., Cerreta, E., 2017. Modeling and simulation framework for dynamic strain localization in elasto-viscoplastic metallic materials subject to large deformations. *International Journal of Plasticity* 88 (Supplement C), 1 – 26.
URL <http://www.sciencedirect.com/science/article/pii/S0749641916301668>
- Nieto-Fuentes, J., Rittel, D., Osovski, S., 2018. On a dislocation-based constitutive model and dynamic thermomechanical considerations. *International Journal of Plasticity* 108, 55 – 69.
URL <http://www.sciencedirect.com/science/article/pii/S0749641918300615>
- Pathak, S., Kalidindi, S. R., 2015. Spherical nanoindentation stress-strain curves. *Materials Science and Engineering: R: Reports* 91 (0), 1–36.
- Pathak, S., Michler, J., Wasmer, K., Kalidindi, S. R., 2012. Studying grain boundary regions in polycrystalline materials using spherical nano-indentation and orientation imaging microscopy. *Journal of Materials Science* 47, 815–823.
- Peirce, D., Asaro, R. J., Needleman, A., 1982. An analysis of nonuniform and localized deformation in ductile single crystals. *Acta metall.* 30, 1087–1119.
- Peirce, D., Asaro, R. J., Needleman, A., 1983. Material rate dependence and localized deformation in crystalline solids. *Acta metall.* 31, 1951–1976.
- Peng, X., Mathew, N., Beyerlein, I., Dayal, K., Hunter, A., 2020. A 3d phase field dislocation dynamics model for body-centered cubic crystals. *Computational Materials Science* 171 (109217).
- Po, G., Huang, Y., Ghoniem, N., 2019. A continuum dislocation-based model of wedge microindentation of single crystals. *Int. J. Plasticity* 114, 72–86.

- Rao, S., Woodward, C., Akdim, B., Antillon, E., Parthasarathy, T., El-Awady, J., Dimiduk, D., 2019. Large-scale dislocation dynamics simulations of strain hardening of ni microcrystals under tensile loading. *Acta Materialia* 164, 171–183.
- Rittel, D., Kidane, A., Alkhader, M., Venkert, A., Landau, P., Ravichandran, G., 2012. On the dynamically stored energy of cold work in pure single crystal and polycrystalline copper. *Acta Materialia* 60 (9), 3719 – 3728.
URL <http://www.sciencedirect.com/science/article/pii/S1359645412002194>
- Rittel, D., Zhang, L., Osovski, S., 2017. The dependence of the taylor-quinney coefficient on the dynamic loading mode. *Journal of the Mechanics and Physics of Solids* 107, 96 – 114.
URL <http://www.sciencedirect.com/science/article/pii/S0022509617301709>
- Rosakis, P., Rosakis, A., Ravichandran, G., Hodowany, J., 2000. A thermodynamic internal variable model for the partition of plastic work into heat and stored energy in metals. *Journal of the Mechanics and Physics of Solids* 48 (3), 581 – 607.
URL <http://www.sciencedirect.com/science/article/pii/S0022509699000484>
- Roy, A., Acharya, A., 2005. Finite element approximation of field dislocation mechanics. *Journal of the Mechanics and Physics of Solids* 53, 143–170.
- Roy, A., Acharya, A., 2006. Size effects and idealized dislocation microstructure at small scales: predictions of a phenomenological model of mesoscopic field dislocation mechanics: Part ii. *Journal of the Mechanics and Physics of Solids* 54, 1711–1743.
- Santos-Guemes, R., Esteban-Manzanares, G., Papdimitriou, I., Segurado, J., Capolungo, L., Llorca, J., 2018. Discrete dislocation dynamics simulations of dislocation- θ' precipitate interaction in al-cu alloys. *Journal of the Mechanics and Physics of Solids* 118, 228–244.
- Shizawa, K., Kikuchi, K., Zbib, H. M., 2001. A strain-gradient thermodynamic theory of plasticity based on dislocation density and incompatibility tensors. *Mats. Sci. Eng. A* 309-310, 416–419.
- Simmons, G., Wang, H. (Eds.), 1971. *Single Crystal Elastic Constants and Calculated Aggregate Properties*. MIT Press.

- Smith, M., 2014. ABAQUS/Standard User's Manual, Version 6.14. Simulia.
- Stainier, L., Ortiz, M., 2010. Study and validation of a variational theory of thermo-mechanical coupling in finite visco-plasticity. *International Journal of Solids and Structures* 47 (5), 705 – 715.
URL <http://www.sciencedirect.com/science/article/pii/S0020768309004478>
- Taylor, G. I., Quinney, H., 1934. The latent energy remaining in a metal after cold working. *Proceedings of the Royal Society of London A: Mathematical, Physical and Engineering Sciences* 143 (849), 307–326.
URL <http://rspa.royalsocietypublishing.org/content/143/849/307>
- Thevamaran, R., Lawal, O., Yazdi, S., Jeon, S.-J., Lee, J.-H., Thomas, E., 2016. Dynamic creation and evolution of gradient nanostructure in single-crystal metallic microcubes. *Science* 354, 312–316.
- Upadhyay, M. V., Capolungo, L., Balogh, L., 2014. On the computation of diffraction peaks from discrete defects in continuous media: comparison of displacement and strain-based methods. *Journal of Applied Crystallography* 47, 861878.
- Vogler, T. J., Clayton, J. D., 2008. Heterogeneous deformation and spall of an extruded tungsten alloy: plate impact experiments and crystal plasticity modeling. *J. Mech. Phys. Solids* 56, 297–335.
- Wu, T.-Y., Bassani, J. L., Laird, C., 1991. Latent hardening in single crystals- i. theory and experiments. *Proc. Roy. Soc. Lond A* 435, 1–19.
- Wu, X. Y., Ramesh, K. T., Wright, T. W., 2003. The coupled effects of plastic strain gradient and thermal softening on the dynamic growth of voids. *International Journal of Solids and Structures* 40, 6633–6651.
- Xue, S., Fan, Z., Lawal, O., Thevamaran, R., Li, Q., Liu, Y., Yu, K., Wang, J., Thomas, E., Wang, H., Zhang, X., 2017. High-velocity projectile impact induced 9r phase in ultrafine-grained aluminium. *Nature Communications* 8 (1), 1653.
- Zaera, R., Rodriguez-Martinez, J., Rittel, D., 2013. On the taylor-quinney coefficient in dynamically phase transforming materials. application to 304 stainless steel. *International Journal of Plasticity* 40, 185 – 201.
URL <http://www.sciencedirect.com/science/article/pii/S0749641912001192>

- Zecevic, M., Knezevic, M., Beyerlein, I. J., Tomé, C. N., 2015. An elasto-plastic self-consistent model with hardening based on dislocation density, twinning and de-twinning: Application to strain path changes in hcp metals. *Materials Science and Engineering: A* 638, 262 – 274.
URL <http://www.sciencedirect.com/science/article/pii/S0921509315004736>
- Zehnder, A. T., 1991. A model for the heating due to plastic work. *Mechanics Research Communications* 18 (1), 23 – 28.
URL <http://www.sciencedirect.com/science/article/pii/009364139190023P>
- Zeng, Y., Hunter, A., Beyerlein, I., Koslowski, M., 2016. A phase field dislocation dynamics model for a bicrystal interface system: An investigation into dislocation slip transmission across cube-on-cube interfaces. *International Journal of Plasticity* 79.
- Zepeda-Ruiz, L. A., Stukowski, A., Oppelstrup, T., Bulatov, V. V., 2017. Probing the limits of metal plasticity with molecular dynamics simulations. *Nature* 550, 492–495.
- Zhu, H. T., Zbib, H. M., Aifantis, E. C., 1995. On the role of strain gradients in adiabatic shear banding. *Acta Mech.* 111 (1/2), 111–124.